Proc. NIPR Symp. Antarct. Geosci., 9, 1–15, 1996

CRUSTAL VELOCITY MODELS OF SHEAR WAVES IN EAST ANTARCTICA BY RECEIVER FUNCTION INVERSION OF BROADBAND WAVEFORMS

Masaki KANAO[1], Atsuki KUBO[1] and Takuo SHIBUTANI[2]

[1]*National Institute of Polar Research, 9–10, Kaga 1-chome, Itabashi-ku, Tokyo 173*
[2]*Disaster Prevention Research Institute, Kyoto University, Gokasho, Uji 611*

Abstract: Receiver functions from teleseismic earthquakes recorded with broadband seismographs at Dumont d'Urville Station (66.7°S, 140.0°E; DRV) and Mawson Station (67.6°S, 62.9°E; MAW), East Antarctica, are inverted for shear wave velocity models of the crust and uppermost mantle beneath the recording stations. The obtained models are compared with the previously obtained ones of Syowa Station (69.0°S, 39.6°E; SYO) to clarify the relationship with regional tectonic history. A crustal velocity model around DRV derived from 18 events indicates a rather sharp Moho at a depth of 38 km and somewhat less fluctuation within the crust. It might have originated in the Early Proterozoic metamorphism in Adélie Land. High velocity zones in the upper crust together with low velocity discontinuity of the mid-crust may also have a relation to past tectono-thermal activity. A crustal velocity model around MAW determined by using 20 events has a very sharp Moho at 42 km depth that might have developed under high pressure and a thickened crust when a metamorphic event occurred around Mac. Robertson Land in the Late Proterozoic ages. Variation in the crustal velocities at MAW is intermediate among the three stations, which may also have been created by the regional metamorphism.

key words: broadband waveforms, teleseismic receiver functions, shear wave velocity, crustal structure, regional metamorphism

1. Introduction

Seismological studies of the velocity structure in the crust and uppermost mantle in and around the Antarctic plate were conducted mainly by surface wave analyses (*e.g.*, EVISON *et al.*, 1960; KOVACH and PRESS, 1961; KNOPOFF and VANE, 1979). In recent years, tomographic models of phase velocities of Antarctica and surrounding oceans have been presented by using broadband seismographs in the southern hemisphere (ROULAND and ROULT, 1992; ROULT *et al.*, 1994). Enderby Land, particularly around the Napier Complex (Fig. 1), where the oldest metamorphic rocks around 400 Ma were found (*e.g.*, ELLIS, 1983; BLACK *et al.*, 1987), has phase velocities higher by 6 per cent than other regions of Antarctica. This oldest craton has a spatial extent about 500 km from the above surface wave analyses, which does not have enough spatial resolution for the detailed discussion of crustal structure. It is, therefore, necessary to obtain smaller scale velocity variations in the Antarctic continent using recently available broadband waveform data of body waves instead of

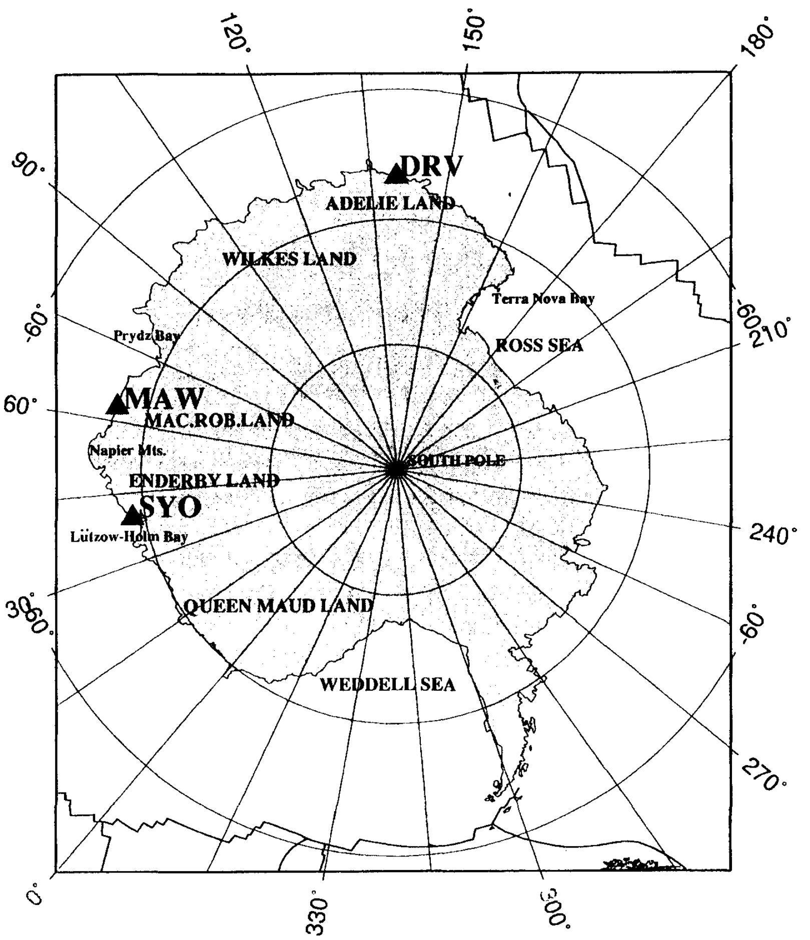

Fig. 1. Map showing the locations of the three stations of SYO, DRV and MAW with several regions concerning the main text.

surface waves.

The broadband seismographs have recently been utilized to determine the shear velocity structure of the crust and uppermost mantle beneath isolated seismic stations. The structure in the Cumberland Plateau, Tennessee (OWENS *et al.*, 1984) shows a thick laminated transition zone between the depths of 40 and 55 km and has a high-velocity middle crustal layer. The result for the Adirondack Highlands, New York (OWENS, 1987) indicates drastic variations in four distinct back-azimuths relating to the existence of a high density layer of granite in the middle crust. On the other hand, the shear wave structure in the island arc of southwest Japan (SHIBUTANI, 1993) and of the Philippines (BESANA *et al*, 1994) have shallower Moho depths of 35 km and 34 km, respectively. However, the structure of a continental collision region, the Qinghai-Tibet Plateau, was revealed to have a very deep transitional Moho from 60 km to 70 km (LUPEI *et al.*, 1994). Some other tectonic areas have also been studied (*e.g.*, OWENS and ZANDT, 1985; VISSER and PAULSSEN, 1993; KIND *et al.*, 1995).

In this study, radial receiver functions (crustal responses) obtained from teleseismic *P*-waveforms recorded with broadband seismographs at Dumont d'Urville Station (66.7°S, 140.0°E; DRV) and Mawson Station (67.6°S, 62.9°E; MAW) are

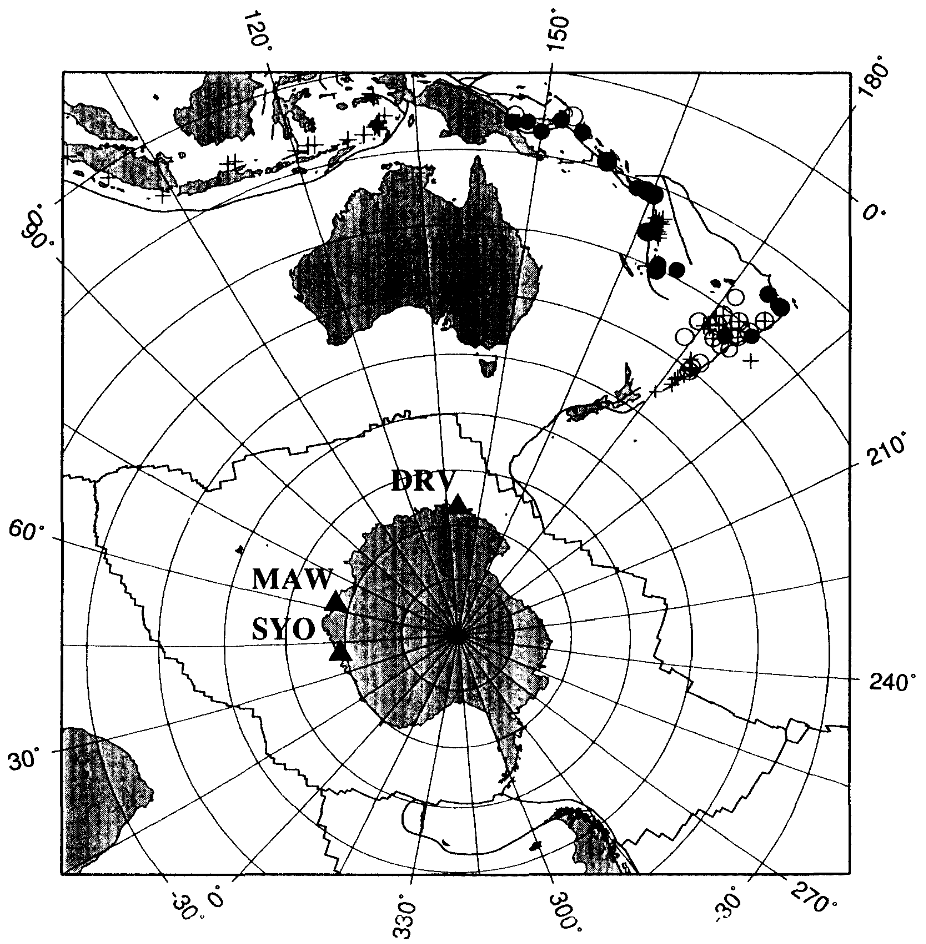

Fig. 2. Map showing the hypocenters used in receiver function inversion analyses together with three stations (solid triangles). (Marks of hypocenters) solid circles; DRV, open circles; MAW, crosses; SYO.

inverted for the shear wave velocity models of the crust and uppermost mantle beneath the metamorphic shield in East Antarctica (Figs. 1, 2). The obtained velocity models are compared with those of Syowa Station (69.0°S, 39.6°E; SYO; KANAO, 1996) to clarify the relationship with the regional metamorphic history from Archaean to Paleozoic ages.

2. Data and Method

In order to derive the structural response (receiver function) beneath the recording station, the source-equalization method (LANGSTON, 1979) is adapted to the P-waveforms of teleseismic events. Crustal response is isolated from that of the instrument and effective seismic source function. Since the receiver functions are sensitive to P-to-S conversions through the interfaces beneath the recording station, the inversion result produces a shear wave velocity structure (OWENS *et al.*, 1984). The observed receiver functions in this study are produced by the following procedures. First, long period noises of more than 0.10–0.20 Hz are eliminated by the high-pass-filtering technique. Then the vertical component is deconvolved from the radial component. The deconvolution is carried out by spectral division with a water level parameter which controls the smallest spectral amplitude allowable for the vertical component. A Gaussian high-cut filter of 1 Hz is also applied to suppress high frequency noise, which corresponds to a thickness larger than 1 km for the sensitive layer. The time window of the receiver functions is set to 40 s from the *P*-arrival in order to eliminate the contamination of other large phases such as *PP* which have different slowness from that of direct *P*-waves.

*Table 1. List of teleseismic earthquakes used in receiver function inversion for all the back-azimuths at two stations (**Inc. angle**; incident angle, **stack_wt.**; weight for stacking of the observed receiver functions). **Mb** denotes the earthquake magnitude determined by USGS.*

Year	Jday	h	m	Lat. deg.	Lon. deg.	Depth km	Mb	Backazimuth deg.	Inc.angle deg.	stack_wt.
DRV		***N=18***								
91	45	19	28	-6.279	154.697	45	5.8	16.73	28.44	0.70
91	96	14	40	-15.008	-175.521	16	5.8	51.94	29.10	0.80
91	287	16	4	-9.094	158.442	23	6.3	21.40	29.23	0.80
91	290	9	11	-15.300	-173.556	36	5.6	54.13	28.95	0.80
91	308	6	30	-6.072	148.198	50	5.7	9.34	28.56	0.60
91	309	7	2	-6.237	146.444	105	5.8	7.36	28.55	0.60
92	44	1	34	-15.894	166.318	10	6.1	31.99	31.02	1.00
92	148	5	19	-11.122	165.239	19	6.3	29.55	29.51	0.90
92	161	0	30	-23.007	-176.365	79	5.7	54.29	31.60	0.80
92	175	4	58	-18.893	172.337	33	5.6	39.90	31.49	1.00
92	206	2	15	-7.036	149.932	43	5.6	11.40	28.84	0.60
92	293	12	8	-19.385	169.593	21	5.7	36.86	31.90	1.00
92	359	0	40	-15.293	-173.128	23	5.9	54.58	28.92	0.80
93	65	3	11	-10.972	164.181	20	6.1	28.31	29.53	0.90
93	137	16	9	-5.343	151.985	17	5.7	13.56	28.27	0.70
93	163	5	51	-11.140	162.937	15	5.5	26.93	29.67	0.80
93	348	6	36	-20.704	-173.451	31	5.5	56.45	30.64	0.80
93	363	7	53	-20.230	169.789	33	6.1	37.37	32.14	1.00
MAW		***N=20***								
90	275	15	14	-24.036	-174.646	9	5.8	128.28	22.53	1.00
90	283	06	02	-23.497	179.029	549	6.0	122.54	22.19	1.00
90	355	05	37	-20.467	-174.161	13	6.1	127.54	21.36	1.00
91	008	22	12	-18.057	-173.534	33	6.1	127.33	20.50	1.00
91	160	07	53	-20.252	-176.218	266	6.1	125.63	21.18	1.00
91	273	00	29	-20.878	-178.591	566	6.3	123.73	21.13	1.00
91	291	17	30	-24.295	-177.561	198	5.8	125.81	22.66	1.00
91	317	11	21	8.361	126.371	36	6.1	62.39	19.43	0.40
91	337	10	41	-26.483	178.715	561	6.0	123.35	23.08	1.00
92	177	06	38	-28.314	-176.716	20	6.1	127.95	24.05	1.00
92	193	10	52	-22.483	-178.413	377	6.2	124.44	21.93	1.00
92	229	10	35	-5.368	146.669	215	6.0	86.32	21.13	0.60
92	243	20	17	-17.918	-178.710	565	5.8	122.61	20.27	1.00
92	294	15	55	-24.453	-176.054	64	5.8	127.19	22.74	1.00
92	296	09	11	-30.227	-177.205	26	6.0	128.22	24.67	1.00
92	298	08	30	-29.536	-177.279	19	5.8	127.91	24.48	1.00
93	004	20	49	-22.055	-174.866	33	5.9	127.43	21.91	1.00
93	131	18	35	7.219	126.570	59	6.1	62.97	19.89	0.40
93	220	08	44	12.982	144.801	59	7.1	77.62	18.16	0.50
93	249	04	04	-4.641	153.231	49	6.2	92.10	20.30	0.70

By applying the above method, receiver functions are obtained at DRV for 18 earthquakes in the period from February 1991 to December 1993 in the back-azimuth range within 00°–60° (Table 1). Hypocenters are restricted to ensure small variations in the incident angles within 5°. The broadband waveform data of velocity signals with a sampling frequency of 20 Hz and 24-bit resolution are obtained through the Internet from the GEOSCOPE data center (ROMANOWICZ *et al.*, 1991). A total of 20 earthquakes with sufficient signal-to-noise ratios are used at MAW to obtain receiver functions. The observation period is from August 1990 to August 1993 with almost the same back-azimuth coverage as DRV. Waveform data with sampling frequency of 20 Hz and 16-bit resolution are utilized from the Australian Seismological Centre of the Australian Geological Survey Organization (AUSTRALIAN SEISMOLOGICAL CENTRE, 1995). Figure 2 shows the hypocenters used in this study together with those of SYO (KANAO, 1996).

Observed radial receiver functions before 10 s and after 40 s from the *P*-arrival for two stations are presented in Figs. 3a, b. Large amplitudes are recognized at DRV from 3 to 6 s after the *P*-arrival in all the back-azimuths. There are several noticeable later phases after the *P*-arrival for all the back-azimuths. The phases around 4–5 s are considered to be the directly converted *Ps* at the Moho. As for MAW, large amplitudes are identified in 4.5–5.0 s corresponding to the Moho *Ps* phases. The intra-crustal converted phases are recognized around 1–2 s and 2.5–3.5 s, which imply mid-crustal velocity discontinuities. In the inversion procedure, we use the weighting-stacked receiver functions for all the original traces to determine shear

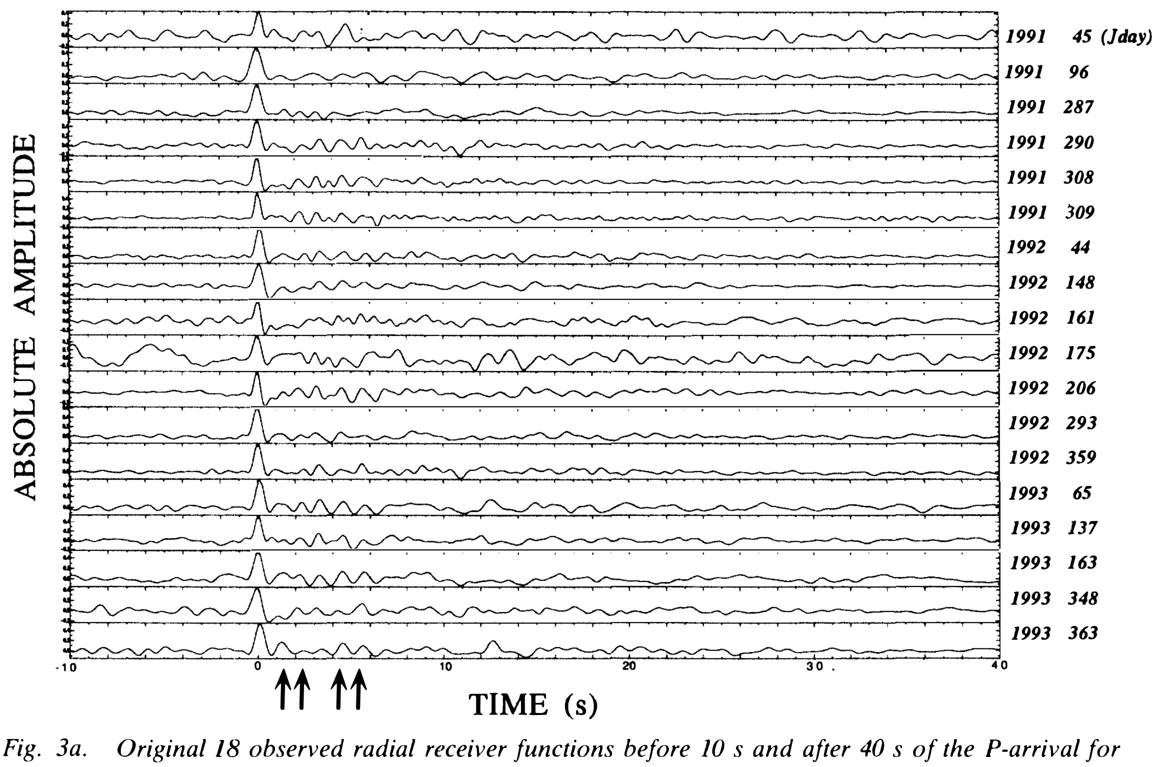

Fig. 3a. Original 18 observed radial receiver functions before 10 s and after 40 s of the P-arrival for weighted-stacking procedures in the 00°–60° back-azimuth at DRV. The predominant intra-crustal P-to-S converted phases are indicated by solid arrows.

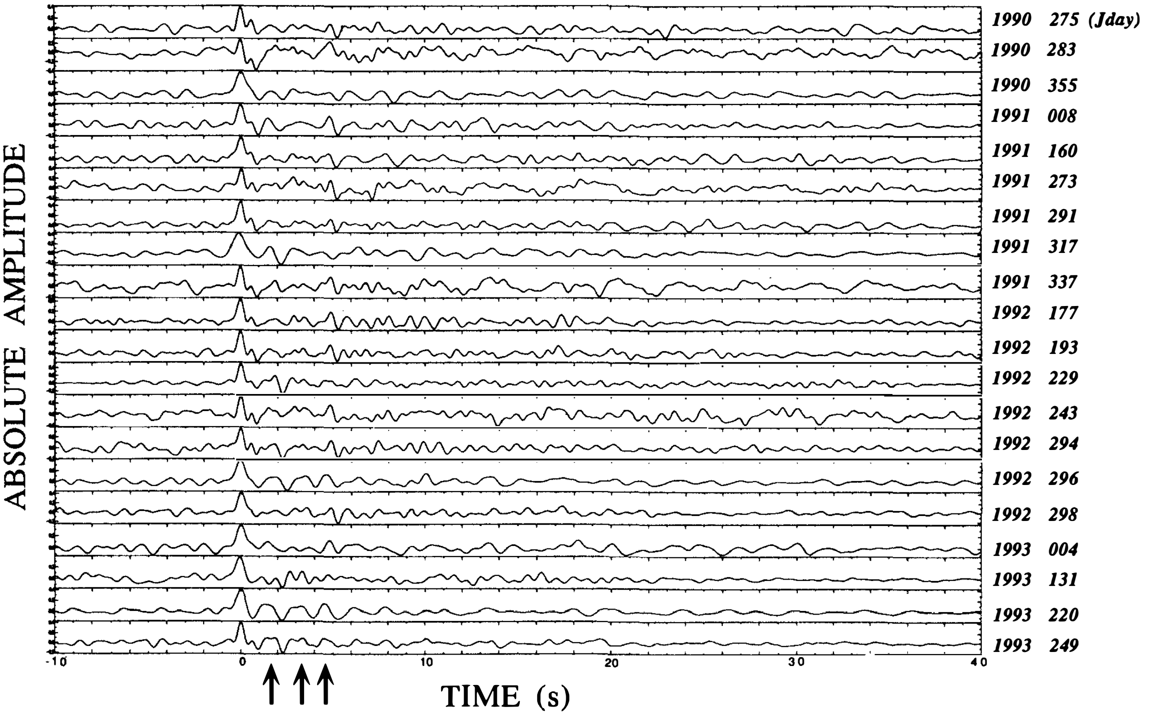

Fig. 3b. Original 20 observed radial receiver functions for weighted-stacking procedures in the 60°–130° back-azimuth at MAW. Same display scheme as Fig. 3a.

velocity models. Weighting-center back-azimuths for the stacking procedure are 30°–40° for DRV and 120°–130° for MAW, where the maximum numbers of original traces are obtained. The stacking-weight for each trace is defined according to the angles between the back-azimuth and the weighting-center back-azimuths (see **stack_wt.** in Table 1). The weighting function for each back-azimuth takes small values when the angle from the weighting-center has a large value. Figs. 4a, b present the weighting-stacked radial receiver functions and standard error bounding for two stations. The incoherent noises can be suppressed by stacking, while the coherent signals are enhanced.

A time domain inversion (Shibutani, 1993) is applied to the weighting-stacked radial receiver functions to determine the velocity model parameterized by 32 thin, flat-lying, homogeneous layers of thickness fixed at 1–2 km. The problem of modeling receiver functions from a flat-layered earth is easily formulated into a linearized time domain inversion. A smoothness constraint in the inversion is implemented by minimizing a roughness norm of the velocity model (Ammon *et al.*, 1990). After examining the trade-off curves between the model roughness and waveform-fit residuals, we select the most suitable pair of the above parameters. The number of iterations, up to 30-times, is conducted in the inversion in order to reduce the waveform-fit residuals to the allowable value, and the most stable solutions are adopted as the final models. The *P*-wave velocity model by the refraction experiments on the northern Mizuho Plateau (Ikami *et al.*, 1984) is adopted as a starting velocity model. In the inversion, we adjust V_p assuming V_p/V_s values of 1.73 for the crust and 1.80 for the uppermost mantle, respectively. Lower- and upper-limits for the shear

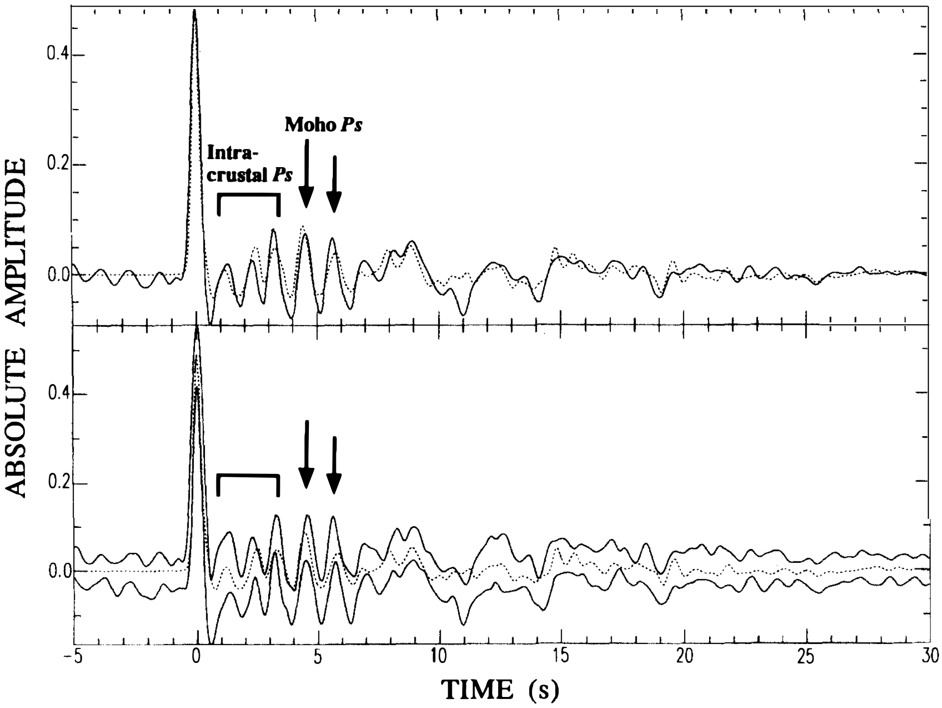

Fig. 4a. *Synthetic radial receiver function (broken traces) compared to observed mean (upper solid trace) and ±1 standard error bounding (lower two solid traces) of weighting-stacked radial receiver functions up to 30 s from the P-arrival in the 00°–60° back-azimuths at DRV. The intra-crustal and Moho Ps phases are indicated by solid arrows.*

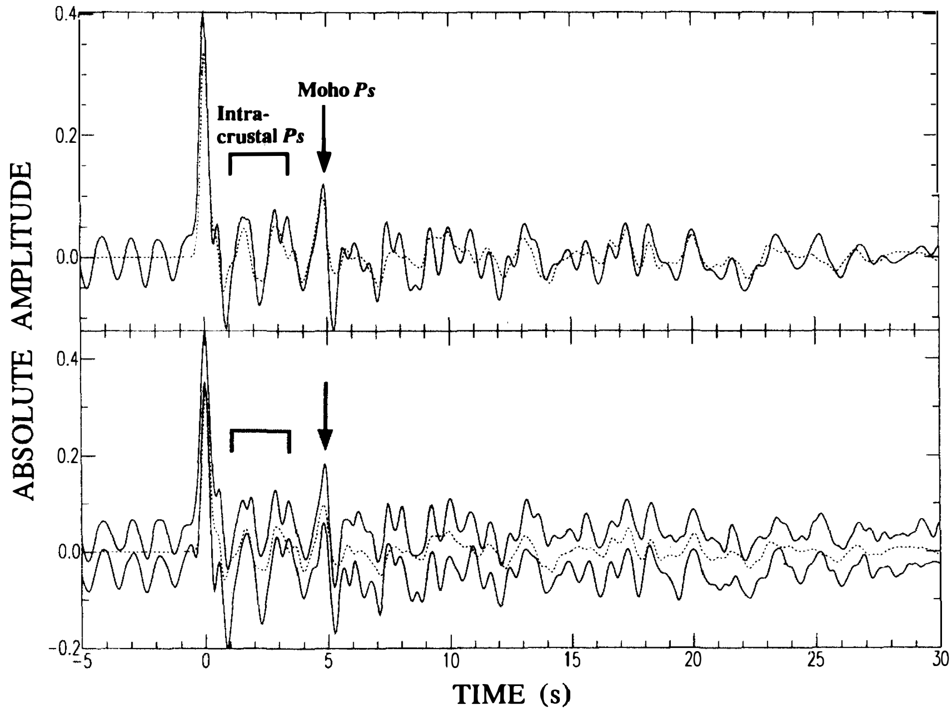

Fig. 4b. *Synthetic radial receiver function compared to observed mean and standard error bounding of weighting-stacked receiver functions in the 60°–130° back-azimuth at MAW. Same display scheme as in Fig. 4a.*

Table 2. List of model parameters in the inversion. The initial velocity model, constraints of upper- and lower-limit of the inversion, ratio of P- to S- wave velocities (V_p/V_s) and the attenuation factor for P- and S- waves (Q_p, Q_s) are shown in 32 layers.

Layer No.	Thickness km	Initial km/s	Lower-limit km/s	Upper-limit km/s	Vp/Vs	Qp	Qs
1	1.00	3.47	2.50	3.80	1.73	60	25
2	2.00	3.53	3.00	3.80	1.73	120	50
3	2.00	3.58	3.00	3.80	1.73	145	60
4	2.00	3.58	3.00	3.80	1.73	157	65
5	2.00	3.61	3.00	3.80	1.73	194	80
6	2.00	3.64	3.00	3.80	1.73	206	85
7	2.00	3.64	3.00	3.80	1.73	206	85
8	2.00	3.70	3.10	4.10	1.73	290	120
9	2.00	3.70	3.10	4.10	1.73	290	120
10	2.00	3.70	3.10	4.10	1.73	290	120
11	2.00	3.70	3.10	4.10	1.73	290	120
12	2.00	3.70	3.10	4.10	1.73	290	120
13	2.00	3.70	3.10	4.10	1.73	290	120
14	2.00	3.70	3.10	4.10	1.73	290	120
15	2.00	3.70	3.10	4.10	1.73	290	120
16	1.00	3.70	3.10	4.10	1.73	290	120
17	1.00	3.84	3.50	4.50	1.73	411	170
18	1.00	3.93	3.50	4.50	1.73	508	210
19	2.00	4.02	3.50	4.50	1.73	726	300
20	2.00	4.02	3.50	4.50	1.73	847	350
21	2.00	4.02	3.50	4.50	1.73	847	350
22	2.00	4.02	3.50	4.50	1.73	847	350
23	2.00	4.41	4.10	4.80	1.80	1360	600
24	2.00	4.41	4.10	4.80	1.80	1360	600
25	2.00	4.41	4.10	4.80	1.80	1360	600
26	2.00	4.41	4.10	4.80	1.80	1360	600
27	2.00	4.47	4.10	4.80	1.80	1360	600
28	2.00	4.47	4.10	4.80	1.80	1360	600
29	2.00	4.47	4.10	4.80	1.80	1360	600
30	2.00	4.47	4.10	4.80	1.80	1360	600
31	2.00	4.47	4.10	4.80	1.80	1360	600
32	2.00	4.47	4.10	4.80	1.80	1360	600

wave velocity in each layer are introduced in the least square method with linear inequality constraints by LAWSON and HANSON (1974). The attenuation models (Q_p, Q_s) in the crust and uppermost mantle are assumed after the values in the Lützow-Holm Bay region (KANAO and AKAMATSU, 1995). However, the Q values scarcely affect the receiver function inversion. The above model parameters used in the inversion are summarized in Table 2.

3. Results

Synthetic radial receiver functions compared with observed mean and ±1 standard error bounding of weighting-stacked receiver functions at two stations are shown in Figs. 4a, b. The synthetic ones are obtained by using the same parameter settings of Gaussian high-cut filter, water level and smoothness constraint as are used in the calculation of observed receiver functions. The waveform fitting between synthetic and observed receiver functions are well in detail and take values within standard error bounding, indicating the adequate inversion procedures with

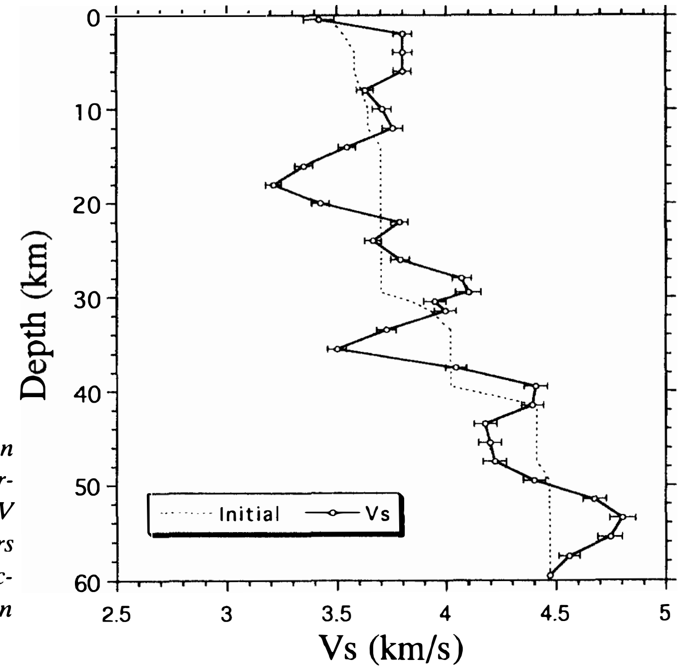

Fig. 5a. Shear wave velocity model down to 60 km depth by receiver function inversion in the 00°–60° back-azimuth at DRV (open circles with solid line). Error bars are ±1 standard errors. The starting velocity model is presented by the thin-broken line.

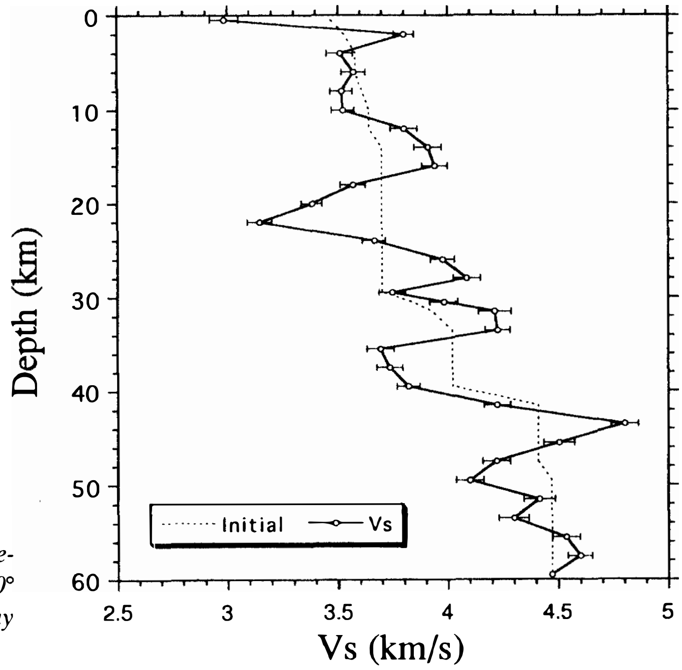

Fig. 5b. Shear wave velocity model by receiver function inversion in the 60°–130° back-azimuth at MAW. Same display scheme as in Fig. 5a.

reasonable smoothness constrained. The later phases after around 7 s have a rather worse waveform fitting compared with those in earlier phases, because of relatively poor signal-to-noise ratio for these later phases in the original receiver functions.

Inverted shear velocity models down to 60 km depth by receiver function inversion at two stations are shown in Figs. 5a, b with the starting velocity models. The resultant velocity model around DRV (Fig. 5a) indicates a sharp Moho at depths of 37–39 km. High velocity zones appear in the upper and lower crustal depths of 3–13 km and 25–31 km, respectively. A low velocity zone appears at depths of 15–22 km, which lies between the above two high velocity zones. There are also low velocities between the lowermost crust and the Moho around 35 km depth. In the uppermost mantle, the velocities fluctuate from rather lower values around 4.2 km/s beneath the Moho to 4.7–4.8 km/s at depths of more than 50 km. High velocity zones of the lower crust, of the Moho and of the uppermost mantle correspond to the three peaks of large amplitudes of directory converted *Ps* phases around 3–6 s in the observed radial receiver functions (see Fig. 4a).

The inverted velocity model around MAW (Fig. 5b) has a very sharp Moho at depths of 41–43 km, which is deeper compared to that of the starting model in the Lützow-Holm Bay region (IKAMI *et al.,* 1984). There are high velocity layers in the upper and lower crustal depths of 3–17 km and 25–33 km; they are likely to be separated by the low velocity layers around 21 km depth. It is also recognized that there are high velocity zones around the Moho, followed by gradually increasing velocities with depth in the uppermost mantle. The above three high velocity layers have an association with three main peaks of large amplitude phases within 5 s after the *P*-arrival in the radial receiver functions (see Fig. 4b). The sharp Moho corresponds to the largest amplitudes of Moho *Ps* phases in 4.5–5.0 s.

4. Discussion

In East Antarctica, shear wave velocity models by receiver function inversion were already obtained around SYO by using teleseismic waveforms from a total of 80 events (KANAO, 1996). Lateral heterogeneity was clarified by analyzing the structures in several azimuthal directions. Crustal velocity variations were large and the Moho was rather sharp at 36–38 km depth in the continental back-azimuths, while they are smooth and transitional in the Lützow-Holm Bay back-azimuths (Fig. 1). Crustal velocity models corresponding to the distinct metamorphic facies terrains were compared in the continental back-azimuths. Around the Terra Nova Bay area (Fig. 1), on the other hand, the Moho depth was estimated by using *Ps* converted phases in the receiver functions from a temporary seismic array data (BONA *et al.,* 1996). Bona et al. found a thinned crust with thickness varying drastically from 17 to 29 km, which implies a transitional zone between East and West Antarctica.

Figure 6a. summarizes the synthetic receiver functions compared with observed standard error bounding of weighting-stacked receiver functions in the two back-azimuth groups at SYO (KANAO, 1996) together with those of DRV and MAW found in this study. The corresponding inverted shear velocity models are presented in Fig. 6b. The numbers of analyzed receiver functions in the two back-azimuth groups at SYO are 26 for 50°–100° and 37 for 120°–160°, respectively. From the figure, the Moho in SYO, DRV and MAW become sharper and deeper in that order, corresponding to sharper and later arrivals of the Moho Ps phases in Fig. 6a. Velocity fluctuation in the inverted crustal models is the largest at SYO, representing the complex structure of the crust. The wide standard error bounding in the stacked receiver functions at SYO, particularly in the 50°–100° back-azimuth, might have caused velocity fluctuation in the inverted model.

The difference between velocity models of two back-azimuth groups at SYO was

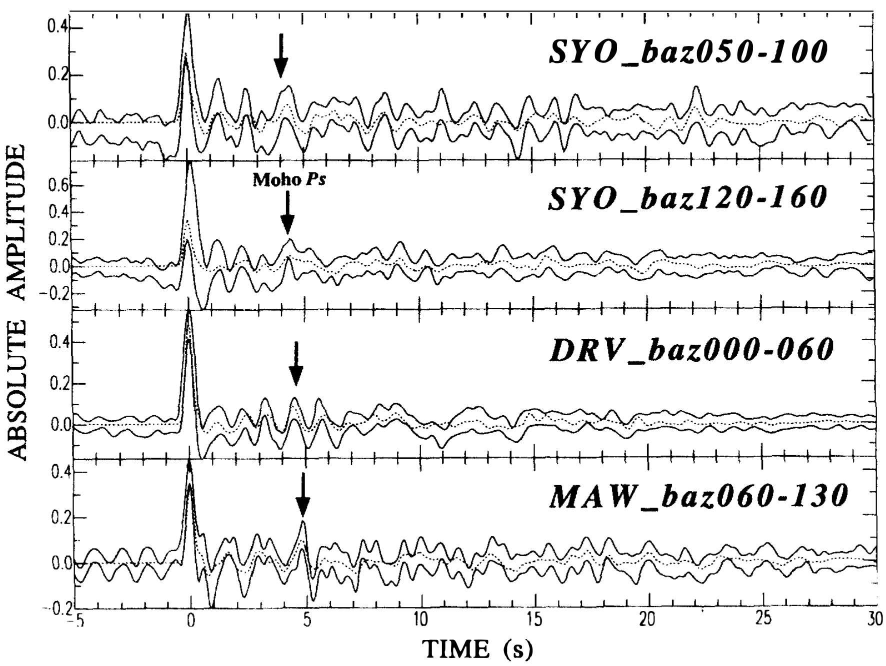

Fig. 6a. Synthetic radial receiver function (broken traces) compared to observed ±1 standard error bounding (solid traces) of weighting-stacked radial receiver functions in the four back-azimuth groups at three stations (SYO; back-azimuths 50°–100° and 120°–160°, DRV; 00°–60°, MAW; 60°–130°). Moho Ps phases are indicated by solid arrows.

considered in relation to lithology by KANAO (1996). As for the continental back-azimuth in 120°–160° corresponding to significant granulite facies, the velocity model has different variations than that for the granulite-amphibolite transitional zone back-azimuths of 50°–100°. The gradual increase of complexity for the crustal velocity models from transitional zone back-azimuth to granulite facies back-azimuth terrain implies increasing metamorphic grade along the NE-SW direction in the Lützow-Holm Bay region. High velocity zones in the upper crust of granulite facies and in the middle-to-lower crust of transitional zone may be consistent with the velocity of the mafic granulite facies found from laboratory data (CHRISTENSEN and MOONEY, 1995). The probable models of crustal evolution to explain this lateral heterogeneity must be related to the compressional stress in the Paleozoic metamorphism of 500 Ma (MOTOYOSHI *et al.*, 1989; HIROI *et al.*, 1991; SHIRAISHI *et al.*, 1994).

DRV is situated in Adélie Land where Early Proterozoic metamorphic rocks have been found (Fig. 1). Rb-Sr biotite and crosscutting pegmatite dates indicate 1543 and 1530 Ma, respectively (BELLAIR and DELBOS, 1962). The metamorphic ages generally become younger from east to west in East Antarctica, together with gradual spreading of the metamorphic area. Regarding tectonic interpretation of the crustal structure around DRV, a rather sharp Moho and somewhat less fluctuation in crustal velocities than those of SYO might have been developed in the older metamorphic age of Adélie Land than in the Lützow-Holm Bay region. High velocity zones in the upper crust together with a low velocity discontinuity in the middle crust might also be

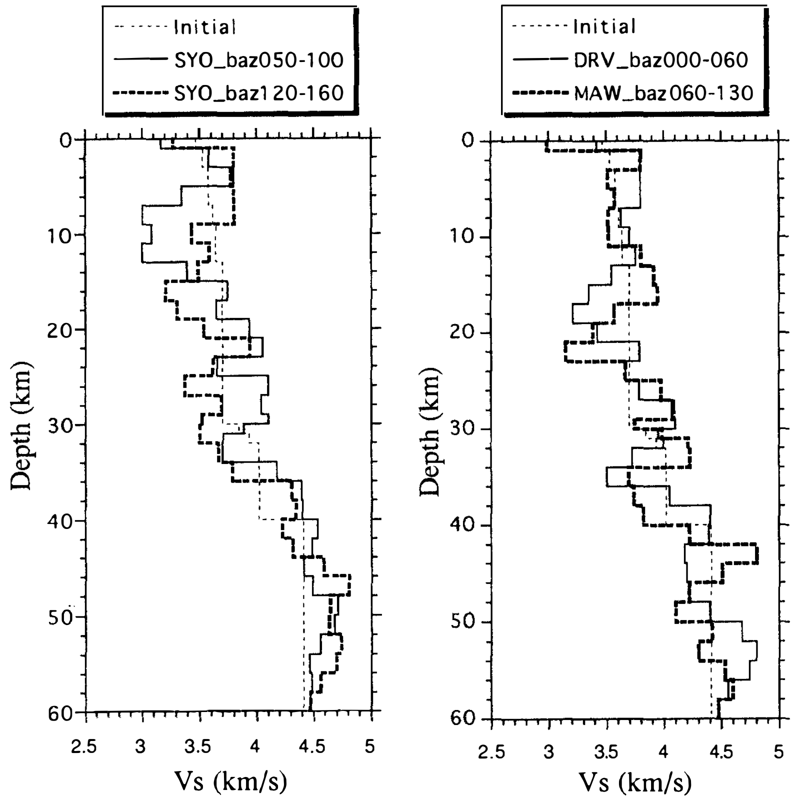

Fig. 6b. Shear wave velocity models down to 60 km depth by receiver function inversion in the four back-azimuth groups at three stations. (left) SYO; back-azimuths 50°–100° (thin solid line) and 120°–160° (thick broken line). (right) DRV; back-azimuth 00°–60° (thin solid line) and MAW; 60°–130° (thick broken line). The starting velocity model is presented by thin broken lines.

related to the Early Proterozoic tectonothermal activity. The absence of later metamorphic events around DRV has caused the crustal velocities to be smoother than those around SYO.

MAW is located in Mac. Robertson Land (Fig. 1) where Late Proterozoic metamorphic granulite facies rocks have been found. Rb-Sr ages are known to have about the same values around 1000 Ma in an east-west trending 500 km wide belt in the Prydz Bay-Prince Charles Mountains-MAW area (TINGEY, 1982; SHERATON and BLACK, 1983) and appear to be continued into the Rayner Complex in Enderby Land (SHERATON *et al.*, 1980, 1987). As for the tectonic interpretation of the crustal structure around MAW, a very sharp and rather deep Moho around 42 km depth may have a relationship with metamorphism of the surrounding Rayner Complex around the Archaean craton of the Napier Complex. The intrusive Mawson charnockites have evidence for a compressional plate margin setting of the Proterozoic mobile belt (YOUNG and ELLIS, 1991). Depletions of heavy rare earth elements in the low-Ti charnockites suggest that garnet was a residual phase in partial melting, which requires high pressures and an overthickened crust. The deep Moho obtained by receiver function inversion seemed to have been formed by this overthickened crust in the compressional plate margin setting. High velocities in the upper crust may be correlated with that in the back-azimuth of 120°–160° at SYO, where in both regions granulite facies gneisses appear on bedrock outcrops. The middle grade variation in the crustal velocity-depth function at MAW, compared to those of DRV and SYO, may also indicate the medium age of the metamorphic history around this area.

In order to making a map of crustal structure in Antarctica, other available broadband data at other seismic stations, such as South Pole Station (90.0°S; SPA), Palmer Station (64.8°S, 64.0°W; PMSA) and Scott Base (77.8°S, 166.8°E; SBA), should be analyzed for comparison. Compilation of the crustal velocity models beneath the seismic stations in West Antarctica and Transantarctic Mountains is important for interpreting the difference of structures in various tectonic regions. The additional analyses of other back-azimuths for each station must clarify the lateral heterogeneity in the continental margin area in the Antarctic shield.

5. Conclusions

Shear velocity models in the crust and uppermost mantle beneath DRV and MAW, East Antarctica, are inverted from teleseismic receiver functions recorded with broadband seismographs. Characteristics for the obtained models and a relationship with regional metamorphic history are summarized as follows:

1) The crustal velocity model of DRV indicates a rather sharp Moho at 38 km depth and somewhat less fluctuation in the velocity-depth function than that of SYO. The structure must have been developed in the Early Proterozoic metamorphism in Adélie Land. High velocity zones in the upper crust together with a low velocity discontinuity in the middle crust must also have a relation to the above tectonothermal activity.

2) The crustal model of MAW has a very sharp and deep Moho around 42 km depth that might have some relationship to a compressional plate margin tectonic setting of the Late Proterozoic mobile belt. The re-working process of the Archaean craton by the Mawson Coast magmatism must had caused high pressures and thickened crust. High velocities in the upper crust may be correlated with that in the granulite facies terrain at SYO.

Acknowledgments

The authors wish to thank Profs. K. Hirahara and T. Iwasaki for their critical reviews and comments for improving the manuscript. They also express their sincere thanks to Profs. K. Kaminuma, K. Shibuya, K. Shiraishi and Y. Motoyoshi in the National Institute of Polar Research for their useful advice on the regional geophysical and geological interpretation. The authors sincerely thank Prof. G. Small in the Australian Seismological Center of the Australian Geological Survey Organization for his grateful effort to make MAW data accessible. They also wish to acknowledge Profs. J. Trampert and G. Roult in the *Ecole et Observatoire de Physique du Globe* for their useful information on DRV data accessibility. Data processing was done on UNIX workstations at the Earth Science Division, National Institute of Polar Research.

References

AMMON, C. J., RANDALL, G. E. and ZANDT, G. (1990): On Nonuniqueness of Receiver Function Inversion. J. Geophys. Res., **95**, 15303–15318.

AUSTRARIAN SEISMOLOGICAL CENTRE (1995): Automatic Data Request Manager Users Guide. Australian Geological Survey Organization.

BELLAIR, P. and DELBOS, L. (1962): Age absolu de la derniere granitisation en Terre Adélie. C. R. Ac. Sc. Paris, **254**, 1465–1466.

BESANA, G. M., SHIBUTANI, T., HIRANO, N., ANDO, M., BAUTISTA, B. C., NARAG I.C. and PUNONGBAYAN, R.S. (1994): The shere wave velocity structure in the uppermost mantle benearth Tagaytay, Philippines using the STS-2 seismometer data (Abstract). Prog. Abs. Seismol. Soc. Jpn., **2**.

BLACK, L., HARLEY, S. L., SUN, S. S. and MCCULLOCH, M. T. (1987): The Rayner complex of East Antarctica: Complex isotopic systematics within a Proterozoic mobile belt. J. Metamor. Geol., **5**, 1–26.

BONA, D., AMATO, A., AZZARA, R., CIMINI, G. B., COLOMBO, D. and PONDRELLI, S. (1996): Constraints on the lithospheric structure benearth the Terra Nova Bay area from teleseismic P to S conversions. submitted to Proc. VII Int. Symp. Antarct. Earth Sci., Siena, Italy.

CHRISTENSEN, N. I. and MOONEY, W. D. (1995): Seismic velocity structure and composition of the continental crust: A global view. J. Geophys. Res., **100**, 9761–9788.

ELLIS, D. J. (1983): The Napier and Rayner Complexes of Enderby Land, Antarctica—contrasting styles of metamorphism and tectonism. Antarctic Earth Science, ed. by R. L. Oliver *et al.* Canberra, Austral. Acad. Sci., 20–24.

EVISON, F. F., INGHAM, C. E., ORR, R. H. and LE FORT, J. H. (1960): Thickness of the Earth's crust in Antarctica and the surrounding oceans. Geophys. J. R. Astron. Soc., **3**, 289–306.

HIROI, Y., SHIRAISHI, K. and MOTOYOSHI, Y. (1991): Late Proterozoic paired metamorphic complexes in East Antarctica, with special reference to the tectonic significance of ultramafic rocks. Geological Evolution of Antarctica, ed. by M. R. A. THOMSON *et al.* Cambridge, Cambridge Univ. Press, 83–87.

IKAMI, A., ITO, K., SHIBUYA, K. and KAMINUMA, K. (1984): Deep crustal structure along the profile between Syowa and Mizuho Stations, East Antarctica. Mem. Natl Inst. Polar Res., Ser. C (Earth Sci.), **15**, 19–28.

KANAO, M. (1996): Variation in the crustal structure of shear waves in the Lützow-Holm Bay region, East Antarctica. Tectonophysics (in press).

KANAO, M. and AKAMATSU, J. (1995): Shere wave Q structure for lithosphere in the Lützow-Holm Bay region, East Antarctica. Proc. NIPR Symp. Antarct. Geosci., **8**, 1–14.

KIND, R., KOSAREV, G. L. and PETERSEN, N. V. (1995): Receiver functions at the stations of the German Regional Seismic Network (GRSN). Geophys. J. Int., **121**, 191–202.

KNOPOFF, L. and VANE, G. (1979): Age of East Antarctica from surface wave dispersion. Pure Appl. Geophys., **117**, 806–815.

KOVACH, R. L. and PRESS, F. (1961): Surface wave dispersion and crustal strucutre in Antarctica and the surrounding oceans. Ann. Geofis., **14**, 211–224.

LANGSTON, C. A. (1979): Structure under Mount Rainier, Washington, inferred from teleseismic body waves. J. Geophys. Res., **84**, 4749–4762.

LAWSON, C. L. and HANSON, R. J. (1974): Solving least squares problems. Englewood Cliffs, Prentice-Hall, **23**, 158–173.

LUPEI, Z., RONGSHENG, Z., WU, F. T., OWENS, T. J. and RANDALL, G. E. (1994): Study on the crust-upper mantle structure of Qinghai-Tibet Plateau by using broadband teleseismic body waveforms. Acta Seismol. Sinica, **37**, 259–266.

MOTOYOSHI, Y., MATSUBARA, S. and MATSUEDA, H. (1989): *P-T* evolution of the granulite-facies of the Lützow-Holm Bay region, East Antarctica. Evolution of Metamorphic Belts, ed. by J. S. DALY *et al.* Oxford, Blackwell Sci. Publ., 325–329 (Geological Society Special Publication, No. 43).

OWENS, T. J. (1987): Crustal structure of the adriondacks determined from broadband teleseismic waveform modeling. J. Geophys. Res., **92**, 6391–6401.

OWENS, T. J. and ZANDT, G. (1985): The response of the continental crust-mantle boundary observed on broadband teleseismic receiver functions. Geophys. Res. Lett., **12**, 705–708.

OWENS, T. J., ZANDT, G. and TAYLOR, S. R. (1984): Seismic evidence for an ancient rift beneath the Cumberland Plateau, Tennessee: A detailed analysis of broadband teleseismic *P* waveforms. J. Geophys. Res., **89**, 7783–7795.

ROMANOWICZ, B., KARCZEWSKI, J. F., CARA, M., BERNARD, P., BORSENBERGER, J., CANTIN, J. M., DOLE, B., FOUASSIER, D., KOENIG, J. K., MORAND, M., PILLET, R. and ROULAND, D. (1991): The geoscope program: Present status and perspectives. Bull. Seismol. Soc. Am., **81**, 243–264.

ROULAND, D. and ROULT, G. (1992): Phase velocity distribution beneath Antarctica and surrounding oceans. Recent Progress in Antarctic Earth Science, ed. by Y. YOSHIDA *et al*. Tokyo, Terra Sci. Publ., 483–487.

ROULT, G., ROULAND, D. and MONTAGNER, J. P. (1994): Antarctia II: Upper-mantle structure from velocities and anisotropy. Phys. Earth Planet. Inter., **84**, 33–57.

SHERATON, J. W. and BLACK, L. P. (1983): Geochemistry of Precambrian gneisses: Relevance for the evolution of the East Antarctic shield. Lithos, **16**, 273–296.

SHERATON, J. W., OFFE, L. A., TINGEY, R. J. and ELLIS, D. J. (1980): Enderby Land, Antarctica—An unusual Precambrian high grade metamorphic terrain. Geol. Soc. Aust., J., **27**, 1–18.

SHERATON, J. W., TINGEY, R. J., BLACK, L. P., OFFE, L. A. and ELLIS, D. J. (1987): Geology of Enderby Land and western Kemp Land, Antarctica. Bull., Bur. Miner. Res., Aust., **223**, 51.

SHIBUTANI, T. (1993): A new method of receiver function inversion for investigating *S* wave velocity structure of the crust and uppermost mantle. Ph. D. thesis, Kyoto University, Kyoto.

SHIRAISHI, K., ELLIS, D. J., HIROI, Y., FANNING, C. M., MOTOYOSHI, Y. and NAKAI, Y. (1994): Cambrian orogenic belt in East Antarctica and Sri Lanka: Implications for Gondwana assembly. J. Geol., **102**, 47–65.

TINGEY, R. J. (1982): The geological evolution of the Prince Charles Mountains-an Antarctic Archaean cratonic block. Antarctic Geoscience, ed. by C. CRADDOCK *et al.* Univ. Wisconsin Press, Madison, 455–464.

VISSER, J. and PAULSSEN, H. (1993): The crustal structure from teleseismic *P*-wave coda-II. Application to data of the NARS array in western Eupore and comparison with deep seismic sounding data. Geophys. J. Int., **112**, 26–38.

YOUNG, D. N. and ELLIS, D. J. (1991): The intrusive Mawson charnockites: evidence for a compressional plate margin setting of the Proterozoic mobile belt. Geological Evolution of Anatrcica, ed. by M. R. A. THOMSON *et al.* Cambridge, Cambridge Univ. Press, 25–31.

(Received March 22, 1996; Revised manuscript accepted July 9, 1996)